RSC Advances

PAPER

View Article Online
View Journal | View Issue

Cite this: *RSC Adv.*, 2024, **14**, 5142

WO$_3$/MIL-125 (Ti) composite material for enhancing the reduction of Cr(VI) under visible light†

Chunhong Jin,[a] Jingchao Liu,[b] Yilin Yin*[a] and Zenghe Li*[a]

Received 2nd January 2024
Accepted 24th January 2024

DOI: 10.1039/d4ra00015c

rsc.li/rsc-advances

In wastewater containing heavy metals, Cr(VI) is a potentially toxic metal, mainly derived from production and processing processes such as textile printing, dyeing, ore mining, battery applications, metal cleaning and electroplating. WO$_3$ is widely used in photocatalytic degradation and reduction, and its utilization rate of visible light is high. However, the rapid recombination of photogenerated electron–hole pairs of WO$_3$ limits its use. In this work, the composite material (WxMy) of WO$_3$ and MIL-125 (Ti) was prepared by the ball milling method, and the catalyst was used to photocatalytically reduce Cr(VI). After using W90M10 as a photocatalyst for 50 min, the reduction rate of Cr(VI) can reach 99.2%, and the reduction rate is 2.3 times that of WO$_3$. After 5 cycles of use, the reduction rate can still reach 91.3%. It is mainly due to the formation of a II-type heterojunction between WO$_3$ and MIL-125 (Ti), which promotes the separation of photogenerated electron–hole pairs, thus improving the efficiency of photocatalytic reduction of Cr(VI).

1. Introduction

With the increasing scarcity of resources and environmental pollution, the treatment of wastewater containing heavy metals has attracted much attention from all walks of life. One of the potentially toxic metals is chromium (Cr). The main sources include textile printing and dyeing, steelmaking, alloy material processing, metal cleaning and electroplating, and other production and processing processes.[1–3] Cr(III) and Cr(VI) are the two most important valence states. Cr(III) is one of the trace elements essential for human health, but Cr(VI) is acutely toxic to most organisms and is carcinogenic.[4] Direct contact with Cr(VI) can cause eye irritation, allergies, dermatitis, and even cancer.[5,6] The World Health Organization limits the concentration of chromium in drinking water to 0.05 mg L^{-1}.[7] Traditional Cr(VI) treatment methods include physical or chemical adsorption, ion exchange, biodegradation, *etc.* However, these treatment methods have high costs and can cause secondary pollution and other problems.[8,9] The photocatalytic reduction method converts Cr(VI) into low-toxic Cr(III) through the photogenerated electrons of the photocatalyst. Its simple process, high efficiency, sustainability, low cost, and environmental friendliness have attracted increasing attention.[10,11]

Tungsten trioxide (WO$_3$), as an n-type semiconductor with good response to sunlight, has received a lot of attention due to its low price, low toxicity, resistance to photo corrosion, stable physical and chemical properties and easy preparation.[12–14] WO$_3$ has a narrow bandgap (2.5–3.5 eV) and a low conduction band (CB) potential.[15] However, the rapid recombination of photogenerated electron–hole pairs in WO$_3$ limits its application in photocatalysis.[16] Feng *et al.* improved the photocatalytic activity of WO$_3$ by doping Fe into WO$_3$ to inhibit the recombination of photogenerated electron–hole pairs.[17] The reduction rate of Cr(VI) increased from 26.2% to 96.1% after Fe doping. Akeem Adeyemi Oladipo inhibit the recombination of photo generated electron hole pairs by preparing WO$_3$/MIL-53 (Fe) heterojunction, and the reduction rate of Cr(VI) increased from 30% to 94%.[18] However, the method of preparing heterojunctions is relatively complex.

Metal–organic frameworks (MOFs) are formed by the self-assembly of metal ions and organic ligands.[19] It has advantages such as ultra-high surface area, adjustable crystal structure, and porous size, but it has low conductivity and rapid recombination of photogenerated electron–hole pairs.[20–22] Li *et al.* prepared a composite material of S–TiO$_2$ and UiO-66-NH$_2$ through ball milling, which improved the utilization rate of visible light by the catalyst.[23] The formed chemical interface can promote the separation of photogenerated electron–hole pairs, thereby improving the photocatalytic activity.

In this work, we prepared WO$_3$/MIL-125 (Ti) composite materials by the ball milling method and applied them for the photocatalytic reduction of Cr(VI). The photocatalytic experiment results show that WO$_3$/MIL-125 (Ti) composite material has a good reduction effect of Cr(VI) and cyclic stability under

---

[a] *Key Laboratory of Environmentally Harmful Chemical Analysis, College of Chemistry, Beijing University of Chemical Technology, Beijing, 100029, China. E-mail: lizh@mail.buct.edu.cn; yinyilin361@163.com*

[b] *Beihang University, Beijing, 100191, China*

† Electronic supplementary information (ESI) available. See DOI: https://doi.org/10.1039/d4ra00015c

visible light. This article will discuss the structure, morphology, and surface chemical composition of WO_3/MIL-125 (Ti) composite materials. We will further explore the mechanism of reducing Cr(VI) in WO_3/MIL-125 (Ti) composite materials through experiments such as free radical capture.

2. Experimental section

2.1 Chemicals

All chemicals used in this study were analytical grade without any purification treatment. Sodium tungstate dihydrate ($Na_2WO_4\cdot 2H_2O$) and tetrabutyl titanate ($C_{16}H_{36}O_4Ti$) were purchased from Aladdin. Vitamin E was purchased from Yuanye Bio-Technology. Hydrochloric acid (HCl), sulfuric acid (H_2SO_4), acetone (CH_3COCH_3), methanol (CH_3OH), isopropyl alcohol (C_3H_8O, IPA), and silver nitrate ($AgNO_3$) were purchased from Beijing chemical plant. Terephthalic acid was purchased from InnoChem. Dibenzoyl dihydrazine, sodium sulfate (Na_2SO_4), sodium hydroxide (NaOH), ethylenediaminetetraacetic acid disodium salt (EDTA-2Na), *N*,*N*-dimethylformamide (DMF), and phosphoric acid (H_3PO_4) were purchased from Fuchen Chemical.

2.2 Preparation of catalysts

2.2.1 WO_3 preparation. WO_3 was prepared based on reported method.[24] 1.15 g of $Na_2WO_4\cdot 2H2O$ was dissolved in 35 mL of deionized water. Then, 35 mL of HCl (35% v/v) was added to the solution with stirring. The above solution was stirred for 30 min. The solution was transferred to a 100 mL Teflon-lined stainless-steel autoclave and heated at 160 °C for 12 h. After cooling down to room temperature, the WO_3 was washed three times with deionized water. Finally, WO_3 was dried in a drying oven at 60 °C for 12 h.

2.2.2 MIL-125 (Ti) preparation. MIL-125 (Ti) was prepared based on reported method.[25] First, 54 mL of DMF and 6 mL of methanol solution were mixed, and 1.56 mL of tetrabutyl titanate was added. The solution was added dropwise to 3 g of terephthalic acid and stirred for 1 h. Then the solution was transferred to a 100 mL Teflon-lined autoclave at 160 °C for 20 h. After cooling down to room temperature, MIL-125 (Ti) was washed with methanol and DMF. Finally, the product was dried in a drying oven at 80 °C for 12 h.

2.2.3 Synthesis of WO_3/MIL-125 (Ti) composites. WO_3/MIL-125 (Ti) was prepared by ball milling. Using 1.5 mm diameter zirconia balls, different mass ratios of WO_3 and MIL-125 (Ti) were ball milled at 3000 rpm for 20 min, and the obtained material was named W*x*M*y*, where W and M represent WO_3 and MIL-125 (Ti), *x* (10, 70, 80, 90, 95) and *y* (90, 30, 20, 10, 5) represent the mass ratio of WO_3 and MIL-125 (Ti) respectively.

2.3 Characterization

The crystal structure of the material was characterized by X-ray diffractometer (XRD, Ultima IV). The crystal morphology and microstructure of the materials were analysed by SEM (ZEISS Gemini SEM 300). The chemical composition and valence state of the sample surface were characterized by a Thermo Scientific K-Alpha ray photoelectron spectrometer (XPS) under Al Kα irradiation. Fourier transform infrared spectroscopy (FTIR) (Thermo Fisher Nicolet 6700) was used to confirm the active groups of the samples. UV-vis diffuse reflectance spectroscopy (DRS) was monitored in the 200–800 nm wavelength range by a UV-3600 UV spectrometer (Shimadzu).

2.4 Photocatalytic measurement

The photocatalytic performance of the composite was evaluated under a 300 W xenon lamp ($l > 420$ nm, CEL-HXF300, Beijing Zhongjiao Jinyuan Technology Co., Ltd) with a UV filter. First, 50 mg of the catalyst was dispersed into 50 mL of Cr(VI) (10 ppm) solution and stirred in the dark for 30 min to reach adsorption–desorption equilibrium. After equilibrium was reached, the solution was illuminated, and 2.5 mL supernatant was taken every 10 min for filtration. The concentration of Cr(VI) was tested at 540 nm with a UV spectrophotometer using the diphenylcarbazide method. The pH of the solution was adjusted using 1 M sulfuric acid and sodium hydroxide.

2.5 Photoelectrochemical measurement

Photoelectrochemical measurements on photocatalysts were performed on a CHI 660E electrochemical system (CH Instruments Inc., Shanghai) using a conventional three-electrode cell (saturated Ag/AgCl electrode, Pt counter electrode, and working electrode). The electrolyte was a 0.1 M Na_2SO_4 aqueous solution. The working electrode was prepared according to the following procedure: evenly disperse 5 mg of catalyst in a mixed solution of 800 mL ethanol, 200 mL deionized water, and 40 mL Nafion. Then, the mixture was dispersed on FTO (1 cm × 3 cm). Under the illumination of a 300 W xenon lamp as the light source, the transient photocurrent response measurements were carried out. Electrochemical impedance spectroscopy (EIS) was tested in the frequency range of 0.1–10^5 Hz under 5 mV sinusoidal alternating current. Mott–Schottky assays were performed in the dark at frequencies of 1000, 1500, and 2000 Hz.[26,27]

3. Results and discussion

3.1 Morphological and structural characterization

The XRD patterns of WO_3, MIL-125 (Ti), and W*x*M*y* were shown in Fig. 1(a). The (002), (020), and (200) crystal planes of WO_3 corresponded to the WO_3 standard card (JCPDS No. 83-0950) at $2\theta = 23.1°$, 23.6°, and 24.4°, respectively.[24] The prepared MIL-

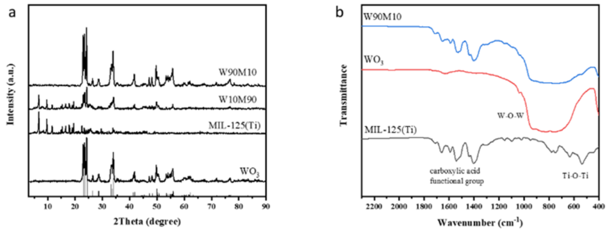

Fig. 1 (a) The XRD patterns and (b) the FTIR spectra of WO_3, MIL-125 (Ti) and W*x*M*y*.

125 (Ti) peak pattern was consistent with the MIL-125 (Ti) peak pattern in the literature, indicating that WO_3 and MIL-125 (Ti) were successfully synthesized.[28] With the increase of MIL-125 (Ti), the WO_3 peak gradually decreased. The MIL-125 (Ti) peak could not be seen in W90M10 because the peak intensity was weak due to the low amount of MIL-125 (Ti) added. This was confirmed by the characteristic peak of MIL-125 (Ti) in W10M90. After ball milling, the crystal plane of the material did not change, and the crystal form remained intact.

The FTIR spectra of WO_3, MIL-125 (Ti), and WxMy were shown in Fig. 1(b). The characteristic peaks in the range of 450–900 cm^{-1} in WO_3 were attributed to the W–O–W stretching vibration, while the characteristic peaks in the range of 400–800 cm^{-1} in MIL-125 (Ti) were attributed to the Ti–O–Ti stretching vibration. The vibrational peaks of the carboxylic acid functional group were observed in the range of 1400–1700 cm^{-1}.[29,30] The structure of the composite material was not damaged by ball milling, and the FTIR results were consistent with those of XRD. The vibration peak of the carboxylic acid functional group was visible in W90M10, which confirmed that the weak intensity of the characteristic peak of MIL-125 (Ti) in XRD was due to the low amount of MIL-125 (Ti) added.

The morphology of the samples was analysed by SEM, and the SEM images of WO_3, MIL-125 (Ti), and W90M10 were shown in Fig. 2. In Fig. 2(a), WO_3 exhibits a nanoscale block structure with a size ranging from 50–200 nm. In Fig. 2(b), MIL-125 (Ti) exhibits a truncated bipyramidal shape, with a size ranging from 5–6 μm. After compounding by ball milling, WO_3 was observed to be compounded on the surface of MIL-125 (Ti), the dimensions of composite materials were 5–6 μm, as shown in Fig. 2(c). From the high-resolution transmission electron microscope (HRTEM) shown in Fig. 2(d–f), it can be observed that after ball milling, WO_3 is tightly bound to the surface of MIL-125 (Ti). The lattice fringes with a crystal plane spacing of 0.384 nm obtained from analysis are consistent with the (002) plane of WO_3.

XPS was employed to measure the elemental composition and binding sites of WO_3, MIL-125 (Ti), and W90M10. As shown in Fig. 3(a), peaks of W, O and Ti were observed in W90M10, indicating the presence of WO_3 and MIL-125 (Ti). After ball

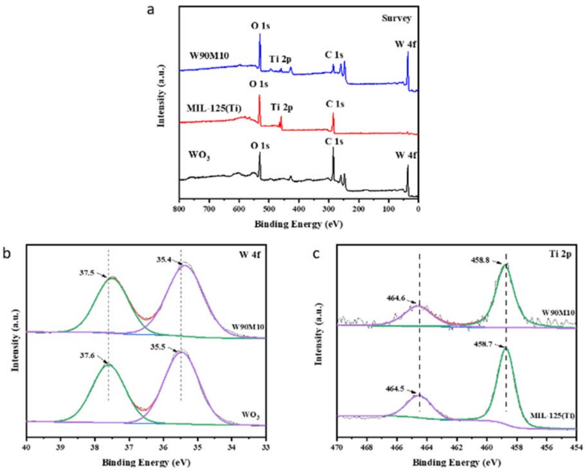

Fig. 3 (a) XPS survey spectra of WO_3, MIL-125 (Ti) and WxMy, (b) HR-XPS spectra of W 4f for WO_3, WxMy, (c) HR-XPS spectra of Ti 2p for MIL-125 (Ti), WxMy.

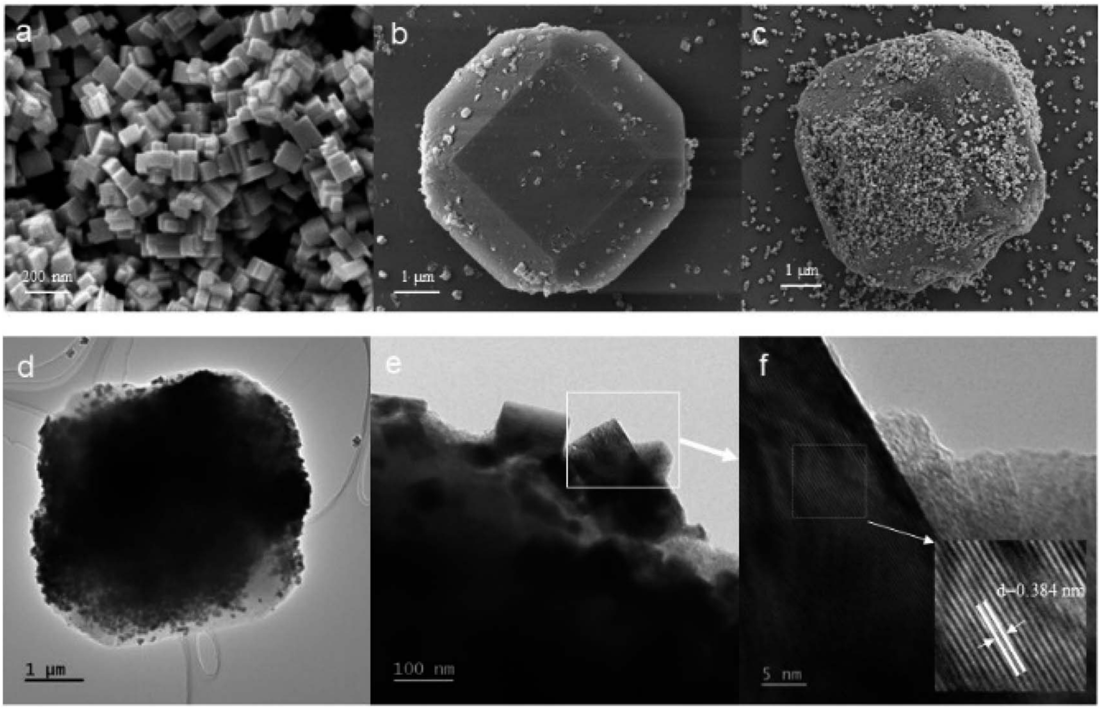

Fig. 2 (a) WO_3, (b) MIL-125 (Ti), (c) SEM images of W90M10, (d–f) TEM images of W90M10.

milling compounding, as shown in Fig. 3(b), the W 4f peak shifted from 37.6 eV and 35.5 eV of the W^{6+} peak in WO_3 to 37.5 eV and 35.4 eV of W90M10.[31] As shown in Fig. 3(c), the Ti 2p peak shifted from 458.7 eV of the Ti $2p_{3/2}$ peak in MIL-125 (Ti) to 458.8 eV of W90M10, and 464.5 eV of the Ti $2p_{1/2}$ peak moved to 464.6 eV of W90M10.[32] These results indicate that electrons were transferred from MIL-125 (Ti) to WO_3. The above results indicate that there is a close contact and certain interaction between WO_3 and MIL-125 (Ti), which is conducive to the separation of photo generated electron hole pairs.

3.2 Photocatalytic performance

The performance of the catalyst was studied by reducing Cr(VI). Fig. 4(a and b) show the reduction effect and rate of the catalyst under visible light irradiation ($l > 420$ nm). During the dark reaction stage, the catalyst showed minimal adsorption of Cr(VI), with MIL-125 (Ti) exhibiting 12% adsorption and WO_3 and W*x*M*y* exhibiting less than 5%. After 50 min of visible light irradiation, the reduction efficiency of Cr(VI) by MIL-125 (Ti) was 24%, while that of WO_3 was 87.4%. The reduction efficiency of Cr(VI) for all composite materials was higher than that of WO_3 and MIL-125 (Ti), with W90M10 exhibiting the highest reduction efficiency of 99.2% and the fastest reduction rate. W90M10 was superior to most reported photocatalysts (Table S3†). The reduction rate of Cr(VI) after simply mixing WO_3 and MIL-125 (Ti) at 90 : 10 is lower than that after ball milling. It shows that the two materials are combined together through ball milling, and there is a close relationship between WO_3 and MIL-125 (Ti).

In order to further demonstrate the photocatalytic effect of W90M10, we conducted reduction of Cr(VI) in the presence of a catalyst under visible light, dark, and only visible light irradiation, as shown in Fig. S2.† In the dark with catalyst and only visible light, Cr(VI) was not reduced, indicating that catalyst and visible light are indispensable conditions for reducing Cr(VI).

The reduction of Cr(VI) is greatly influenced by the pH of the solution due to the different forms of Cr(VI) present at different pH values. The reaction of Cr(VI) at different pH values follows eqn (1) in an acidic environment and eqn (2) in an alkaline environment.

$$Cr_2O_7^{2-} + 14H^+ + 6e^- \rightarrow 2Cr^{3+} + 7H_2O \tag{1}$$

$$CrO_4^{2-} + 4H_2O + 3e^- \rightarrow Cr(OH)_3 + 5OH^- \tag{2}$$

The effect of different pH values on the reduction of Cr(VI) is shown in Fig. 4(c). The best reduction efficiency of Cr(VI) was achieved at a pH of 2. The presence of abundant H^+ ions can promote the reduction of Cr(VI), and the reduction efficiency and rate increase as the pH decreases. When the solution is in an alkaline state, the $Cr(OH)_3$ generated on the catalyst surface will cover the reaction active sites of the catalyst, leading to a decrease in the reduction efficiency of Cr(VI).

W90M10 exhibited the highest photocatalytic efficiency under visible light, and therefore was selected for the reusability experiments. As shown in Fig. 4(e), the repeatability of W90M10 did not decrease significantly after 5 cycles. After 5 trials, 91.3% of Cr(VI) could still be reduced within 50 minutes.

3.3 Enhanced photocatalytic activity mechanism

Fig. 5(a and b) shows the UV-vis DRS and E_g plots of WO_3, MIL-125 (Ti), and W90M10. The bandgap energy of the samples was evaluated using the Tauc curve: $(\alpha h\nu) = A(h\nu - E_g)^{n/2}$, where α, E_g, h, n and A are the absorption coefficient, bandgap energy,

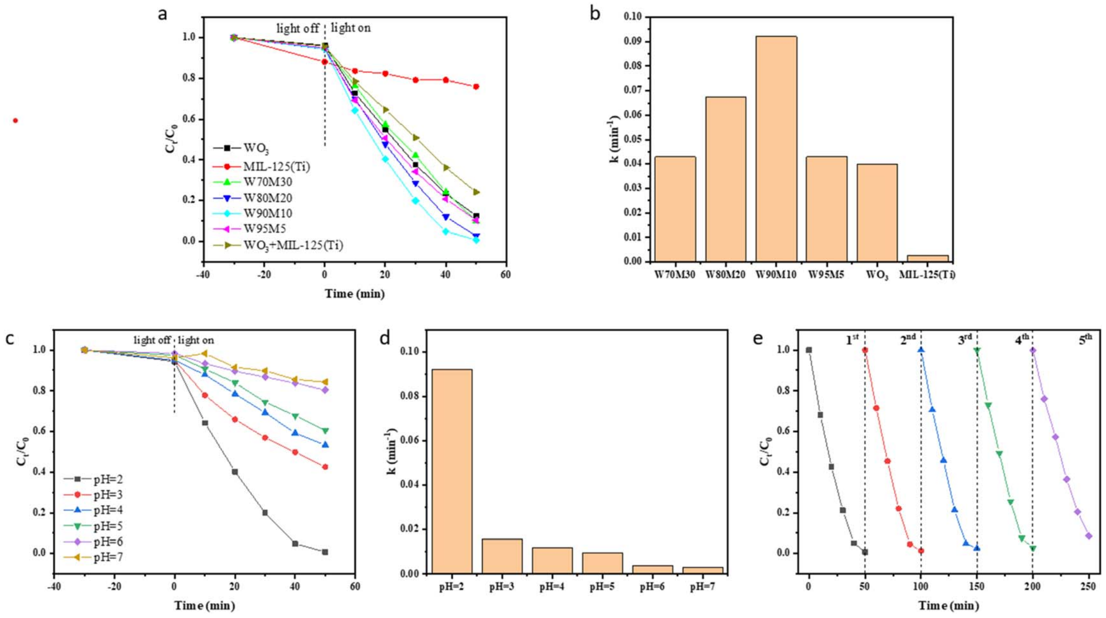

Fig. 4 (a) Photocatalytic reduction efficiency and (b) rate constant *k* of Cr(VI) with different composite ratios of catalysts; (c) photocatalytic reduction efficiency and (d) rate constant *k* of Cr(VI) at different pH; (e) cyclic test of Cr(VI) reduction by W90M10 under visible light catalysis.

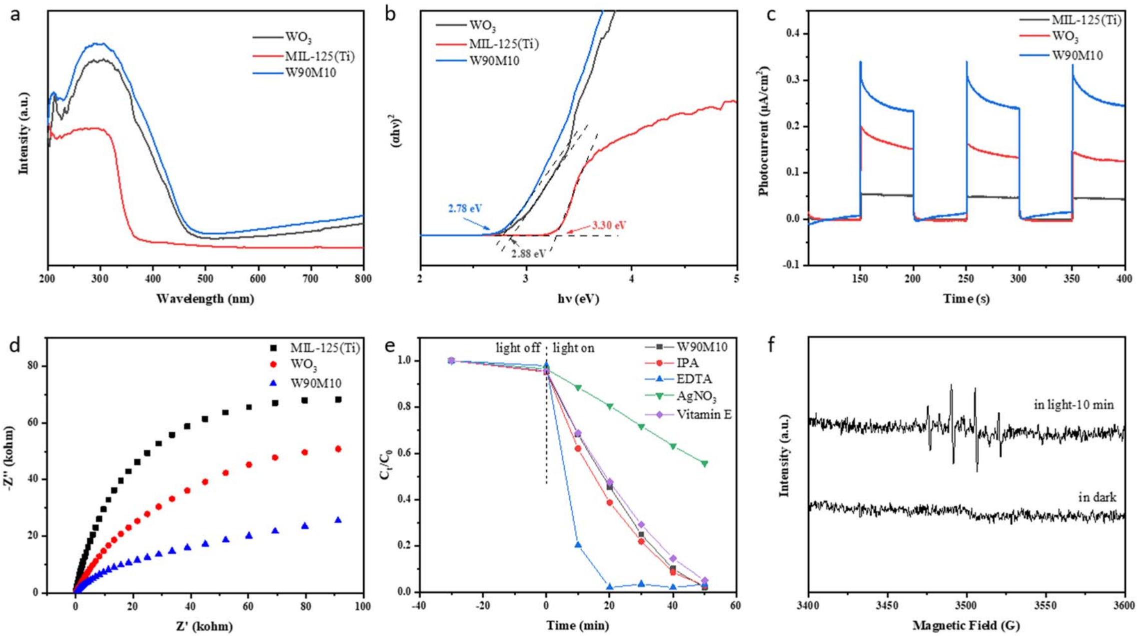

Fig. 5 (a) UV-vis DRS and (b) E_g plots; (c) photocurrent responses and (d) EIS Nyquist plots of WO_3, MIL-125 (Ti) and W90M10; (e) free radical capture experiment for Cr(VI) reduction, (f) DMPO spin-trapping ESR technology for detection of ·OH.

Planck's constant, optical frequencies, and constants.[33,34] The band gaps of WO_3 and MIL-125 (Ti) were 2.88 eV and 3.30 eV, respectively. The band gap of W90M10 was close to that of WO_3, which was 2.78 eV. By ball milling, WO_3 and MIL-125 (Ti) are tightly bonded, resulting in a red shift in the light absorption band of W90M10 and a narrower band gap. This indicates that W90M10 has good photocatalytic performance under visible light.

The separation of e^-/h^+ was further confirmed through photocurrent measurement and electrochemical impedance spectroscopy (EIS). The photocatalytic activity was found to increase with the photocurrent intensity. A smaller radius of the EIS diagram indicates stronger electronic conductivity. As shown in Fig. 5(c), the photocurrent intensity followed the order of W90M10 > WO_3 > MIL-125 (Ti), with W90M10 exhibiting the highest intensity and no significant change after three cycles. In Fig. 5d, the radius followed the order of W90M10 < WO_3 < MIL-125 (Ti), indicating that W90M10 has the fastest transfer of photogenerated carriers.

3.4 The photocatalysis mechanism

The flat band potentials (E_{FB}) of pristine WO_3 and MIL-125 (Ti) were determined from the Mott–Schottky diagrams. Fig. S3† shows that the slopes of WO_3 and MIL-125 (Ti) are both positive, indicating that they are both n-type semiconductors. The flat band potentials of WO_3 and MIL-125 (Ti) were approximately −0.38 eV *vs.* Ag/AgCl (−0.18 eV *vs.* NHE) and −0.90 eV *vs.* Ag/AgCl (−0.70 eV *vs.* NHE), respectively. For n-type semiconductors, the E_{FB} lies approximately 0.1 eV above the E_{CB}.[21] Therefore, the E_{CB} of WO_3 and MIL-125 (Ti) were calculated to be about −0.28 eV and −0.80 eV (*vs.* NHE), respectively. Using the formula $E_g = E_{VB} - E_{CB}$ and the value of E_g, the calculated E_{VB} of WO_3 and MIL-125 (Ti) were 2.60 eV and 2.50 eV (*vs.* NHE), respectively.

To further investigate the mechanism of the photocatalytic reaction, a free radical trapping experiment was conducted using isopropanol (IPA), EDTA-2Na, silver nitrate ($AgNO_3$), and vitamin E to capture ·OH, h^+, e^-, and $\cdot O_2^-$.[35] Upon the addition of $AgNO_3$, the reduction rate of Cr(VI) significantly decreased from 99.2% to 44.2%, indicating that e^- played a major role in the reduction of Cr(VI) (Fig. 5e). Upon the addition of EDTA-2Na, the reduction rate of Cr(VI) was accelerated, suggesting that the separation of e^-/h^+ could be promoted, thereby accelerating the reduction of Cr(VI). Upon the addition of IPA, the reduction rate of Cr(VI) slightly increased, but the final reduction rate did not change significantly, indicating that ·OH was not the main reactive species. Upon the addition of vitamin E, the photocatalytic efficiency did not change significantly.

The capture of ·OH using DMPO *via* electron spin resonance (ESR) further demonstrates the reactive species generated during the photocatalytic process. Fig. 5(f) shows the ESR signal detected in the dark state and after 10 minutes of illumination. No signal peak of ·OH was found in the dark state. The signal peak of ·OH was detected after 10 min of illumination, but the intensity was weak, indicating that less ·OH was produced. Corroborated with the conclusion of the free radical capture experiment.

$$WO_3/MIL-125(Ti) + h\nu \rightarrow MIL-125(Ti)(h^+) + WO_3(e^-) \quad (3)$$

$$Cr(VI) + e^- + H^+ \rightarrow Cr(III) + H_2O \quad (4)$$

$$H_2O + h^+ \rightarrow H^+ + OH^- \quad (5)$$

$$Cr(V) + h^+/\cdot OH \rightarrow Cr(VI) + OH^- \quad (6)$$

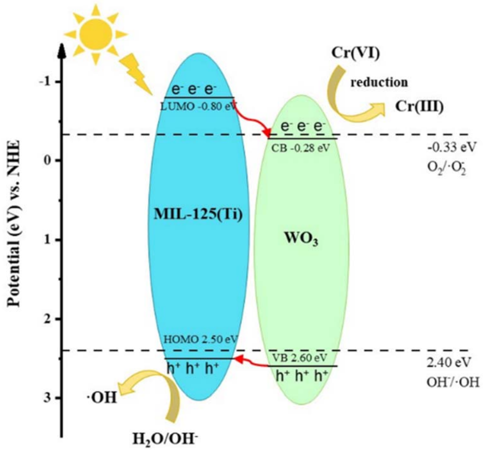

Fig. 6 Schematic diagram of photocatalytic reduction of Cr(VI) by WO_3/MIL-125 (Ti) composite.

Based on the above analysis, we proposed the photocatalytic mechanism of type-II heterojunction, as shown in Fig. 6. When irradiated with a xenon lamp, the electrons of WO_3 and MIL-125 (Ti) are excited, producing photogenerated electrons and holes. The potential of the E_{CB} of WO_3 (−0.28 eV *vs.* NHE) is more negative than the potential of Cr(VI)/Cr(III) (+1.05 eV *vs.* NHE), Cr(VI) is reduced to Cr(III) on the CB of WO_3. Since the potential of E_{VB} of MIL-125 (Ti) (2.50 eV *vs.* NHE) is more positive than that of $OH^-/\cdot OH$ (2.40 eV *vs.* NHE), H_2O/OH^- reacts with h^+ at VB of MIL-125 (Ti) to generate $\cdot OH$.[36,37]

4. Conclusions

This study successfully prepared WO_3/MIL-125 (Ti) composite material using the ball-milling method. The W90M10 composite material exhibited significantly higher photocatalytic reduction ability for Cr(VI) compared to WO_3, MIL-125 (Ti), and other composite materials, with a reduction rate of 99.2% within 50 minutes. After 5 cycles, it maintained a reduction rate of 91.3%. The positions of CB and LUMO were measured using Mott–Schottky curves, and the mechanism of photocatalytic Cr(VI) was speculated through free radical capture experiments. The improved photocatalytic performance of the W90M10 composite material is due to the successful preparation of the composite material, which leads to effective separation of photo-generated electron–hole pairs. This work further demonstrates that composite materials can be prepared using the ball-milling method to improve their photocatalytic performance.

Conflicts of interest

There are no conflicts to declare.

Acknowledgements

The authors would like to thank Professor Zenghe Li for financial support and guidance.

References

1 M. Naimi-Joubani, M. Shirzad-Siboni, J.-K. Yang, M. Gholami and M. Farzadkia, *J. Ind. Eng. Chem.*, 2015, **22**, 317–323.
2 Y. Hua, C. Hu, M. Arif, S.-m. Chen, M. Zhang and X. Liu, *J. Alloys Compd.*, 2022, **908**, 164488.
3 C. Wang, X. Du, J. Li, X. Guo, P. Wang and J. Zhang, *Appl. Catal., B*, 2016, **193**, 198–216.
4 W. Liu, Z. Guo, Z. Jin, D. Chen, T. Lu, P. Jia and H. Xing, *Catal. Sci. Technol.*, 2022, **12**, 2176–2183.
5 X. Wang, Z. Cao, B. Du, Y. Zhang and R. Zhang, *Composites, Part B*, 2020, **183**, 107685.
6 G. Li, Y. Wu, M. Zhang, B. Chu, W. Huang, M. Fan, L. Dong and B. Li, *Ind. Eng. Chem. Res.*, 2019, **58**, 8979–8989.
7 L. W. Duresa, D. Kuo, K. E. Ahmed, M. A. Zeleke and H. Abdullah, *New J. Chem.*, 2019, **43**, 8746–8754.
8 L. Zhang, C. Chuaicham, V. Balakumar and K. Sasaki, *J. Photochem. Photobiol., A*, 2022, **429**, 113909.
9 L. Zhao, L. Guo, Y. Tang, J. Zhou and B. Shi, *Ind. Eng. Chem. Res.*, 2021, **60**, 13594–13603.
10 J. Dong, J. Hu, A. Liu, J. He, Q. Huang, Y. Zeng, W. Gao, Z. Yang, Y. Zhang, Y. Zhou and Z. Zou, *Catal. Sci. Technol.*, 2021, **11**, 6271–6280.
11 X. Wei, C. Wang, Y. Li, P. Wang and Q. Wei, *Chemosphere*, 2021, **280**, 130734.
12 Y. Jia, X. Zhang, R. Wang, J. Yuan, R. Zheng, J. Zhang, F. Qian, Y. Chen, M. Zhang and L. Guo, *Appl. Surf. Sci.*, 2023, **618**, 13.
13 Y. Yang, Y. Li, X. Ma, L. Xie, D. Lv, L. Jiang, J. He, D. Chen and J. Wang, *Catal. Sci. Technol.*, 2023, **13**, 5599–5609.
14 O. Samuel, M. H. D. Othman, R. Kamaludin, O. Sinsamphanh, H. Abdullah, M. H. Puteh and T. A. Kurniawan, *Ceram. Int.*, 2022, **48**, 5845–5875.
15 S. Nazari, E. Asgari, A. Sheikhmohammadi, S. A. Mokhtari and H. Alamgholiloo, *J. Environ. Chem. Eng.*, 2023, **11**, 13.
16 M. H. Thanh Tung, T. T. Thu Phuong, N. T. Phuong Le Chi, D. M. The, N. T. Quoc, D. T. Khan, T.-D. Pham, N. V. Khoa, T. T. Thu Hien and N. T. Dieu Cam, *Ceram. Int.*, 2023, **49**, 10881–10888.
17 M. Feng, Y. Liu, Z. Zhao, H. Huang and Z. Peng, *Mater. Res. Bull.*, 2019, **109**, 168–174.
18 A. A. Oladipo, *Process Saf. Environ. Prot.*, 2018, **116**, 413–423.
19 B. Xu, Z. Chen, B. Han and C. Li, *Catal. Commun.*, 2017, **98**, 112–115.
20 F. Zhao, Y. Liu, S. B. Hammouda, B. Doshi, N. Guijarro, X. Min, C.-J. Tang, M. Sillanpää, K. Sivula and S. Wang, *Appl. Catal., B*, 2020, **272**, 119033.
21 K. Shi, F. Qiu, J. Wang, P. Wang, H. Li and C. Wang, *Sep. Purif. Technol.*, 2023, **309**, 122991.
22 L. Wang, K. Zhang, J. Qian, M. Qiu, N. Li, H. Du, X. Hu, Y. Fu, M. Tan, D. Hao and Q. Wang, *Chemosphere*, 2023, **344**, 140277.
23 Y. Li, X. Wang, C. Wang, H. Fu, Y. Liu, P. Wang and C. Zhao, *J. Hazard. Mater.*, 2020, **399**, 123085.
24 G. Chen, Q. Wang, Z. Zhao, L. Gao and X. Li, *Environ. Sci. Pollut. Res.*, 2020, **27**, 15103–15112.

25 X. Han, X. Yang, G. Liu, Z. Li and L. Shao, *Chem. Eng. Res. Des.*, 2019, **143**, 90–99.

26 J. Zhang, X. Gao, W. Guo, Z. Wu, Y. Yin and Z. Li, *RSC Adv.*, 2022, **12**, 6676–6682.

27 X. Yu, J. Huang, J. Zhao, S. Liu, D. Xiang, Y. Tang, J. Li, Q. Guo, X. Ma and J. Zhao, *Chem. Eng. J.*, 2021, **403**, 126359.

28 X. Cheng, X. Dao, S. Wang, J. Zhao and W. Sun, *ACS Catal.*, 2021, **11**, 650–658.

29 Y. Zhang, F. Mao, Y. Liu, X. Wu, C. Wen, S. Dai, P. Liu and H. Yang, *Sci. China Mater.*, 2022, **65**, 1237–1244.

30 J. Wang, F. Qiu, P. Wang, C. Ge and C. Wang, *J. Cleaner Prod.*, 2021, **279**, 123408.

31 R. Xie, K. Fang, Y. Liu, W. Chen, J. Fan, X. Wang, Y. Ren and Y. Song, *J. Mater. Sci.*, 2020, **55**, 11919–11937.

32 Q. Hu, S. Yin, Y. Chen, B. Wang, M. Li, Y. Ding, J. Di, J. Xia and H. Li, *Colloids Surf., A*, 2020, **585**, 124078.

33 X. Lian, Z. Huang, Y. Zhang, Z. Chen, P. Meidl, X. Yi and B. Xu, *Chemosphere*, 2023, **313**, 137351.

34 Q. Zhao, S. Liu, S. Chen, B. Ren, Y. Zhang, X. Luo and Y. Sun, *Chem. Phys. Lett.*, 2022, **805**, 139908.

35 X. Yi, S. Ma, X. Du, C. Zhao, H. Fu, P. Wang and C. Wang, *Chem. Eng. J.*, 2019, **375**, 121944.

36 S. Habi Ben Hariz, H. Lahmar, G. Rekhila, A. Bouhala, M. Trari and M. Benamira, *J. Photochem. Photobiol., A*, 2022, **430**, 113986.

37 D. Chen, X. Yi, C. Zhao, H. Fu, P. Wang and C. Wang, *Chemosphere*, 2020, **245**, 125659.